PROCEEDINGS OF SPIE

SPIEDigitalLibrary.org/conference-proceedings-of-spie

Mid-IR photothermal sensing of liquids for trace analysis

Giovanna Ricchiuti, Alicja Dabrowska, Davide Pinto, Georg Ramer, Bernhard Lendl

Giovanna Ricchiuti, Alicja Dabrowska, Davide Pinto, Georg Ramer, Bernhard Lendl, "Mid-IR photothermal sensing of liquids for trace analysis," Proc. SPIE 12428, Photonic Instrumentation Engineering X, 124280N (8 March 2023); doi: 10.1117/12.2649811

SPIE.

Event: SPIE OPTO, 2023, San Francisco, California, United States

Downloaded From: https://www.spiedigitallibrary.org/conference-proceedings-of-spie on 10 Mar 2023 Terms of Use: https://www.spiedigitallibrary.org/terms-of-use

Mid-IR photothermal sensing of liquids for trace analysis

Giovanna Ricchiuti[1], Alicja Dabrowska[1], Davide Pinto[1], Georg Ramer[1], Bernhard Lendl[1]
[1]Institute of Chemical Technologies and Analytics, TU Wien, Getreidemarkt 9/164, 1060 Vienna, Austria

ABSTRACT

Photothermal Spectroscopy (PTS) is an indirect analytical technique in which the optical signal is directly proportional to the laser emission intensity. This direct dependence on the laser power means that - in contrast to more conventional transmission-absorption techniques - PTS fully benefits from the high power of novel tunable mid-infrared laser sources such as Quantum Cascade Lasers (QCLs). In particular, QCLs equipped with an external cavity (EC) allow broad tunability which can be exploited in the detection of liquids identified by broad absorption bands. To achieve high sensitivity in PTS it is also important to choose a sensitive mode of transducing photothermal signal. Among the PTS transduction techniques photothermal interferometry (i.e. the detection of the phase change resulting from sample heating) stands out due to its high sensitivity.

In this work, we use an EC-QCL in a photothermal interferometry PTS setup for trace water detection. We employ a HeNe laser-based Mach-Zehnder Interferometer (MZI) with liquid flow-cells inserted in the two arms. An EC-QCL emitting in the range of 1570-1730 cm^{-1} is arranged co-linear to the analyte arm of the interferometer and used to target the bending mode (ν_2 ~ 1645 cm^{-1}) of water molecules in different matrices. Highest linearity and sensitivity are ensured by locking the MZI at its quadrature point via an active-feedback loop. Fluctuations and drifts are further minimized by means of temperature stabilization. When benchmarking the system against commercial FTIR spectrometers it is shown to be in excellent agreement with regards to band shapes, band positions and relative intensities and to compare favorably in terms of sensitivity. Achieved limits of detection (LODs) for water in chloroform and jet-fuel are in the low ppm range. Higher LODs orders of magnitude were obtained indeed for the case of water in ethanol. An analysis of the matrix influence on the PTS signal's strength has been carried out. Results show how the choice of the matrix dramatically influences limits of detection and limits of quantification (LOQs).

Keywords: photothermal spectroscopy, liquid sensing, quantum cascade laser, Mach-Zehnder Interferometer, mid-IR, water detection

1. INTRODUCTION

Mid-infrared spectroscopy is known as a powerful process analytical technology tool for qualitative and quantitative analysis of chemicals (e.g. solid, gas and liquids). Over the last decade, infrared spectroscopy has widely employed quantum cascade lasers (QCLs) as light sources. These sources are characterized by high power, broad tunability across the mid-IR and high brilliance enabling many new mid-IR spectroscopy sensing schemes.[1] In contrast to conventional direct absorption schemes that rely on detecting minute difference in intensity reduction from a high baseline and thus do not fully benefit from QCLs' high power, photothermal spectroscopy (PTS) uses an indirect detection approach, meaning that the PTS signal is directly proportional to the laser emission intensity. Increasing the power of the laser thus means that signal-to-noise ratios increase and in turn the sensitivity is enhanced. The PTS signal is generated by a photoinduced change in the sample thermal state. Its amplitude can be expressed as per[2,3]:

$$\text{PTS signal} \propto \Delta\text{T} \propto \frac{P(\tilde{\nu})\,\alpha(\tilde{\nu})\,L}{\rho C_P V f_{mod}} \tag{1}$$

where $P(\tilde{\nu})$ is the laser power of the excitation source, $\alpha(\tilde{\nu})$ is the analyte linear absorption coefficient, L is the optical pathlength, ρ is the density and C_P is the heat capacity of the sample, f_{mod} is the applied modulation frequency and V is the volume of the beam when interacting with the sample.[2] The thermal gradient ΔT can be probed through the resulting sample refractive index change (Δn). The challenge lies in detecting Δn at high sensitivity. To do that, we exploit a

Photonic Instrumentation Engineering X, edited by Lynda E. Busse, Yakov Soskind, Proc. of SPIE
Vol. 12428, 124280N · © 2023 SPIE · 0277-786X · doi: 10.1117/12.2649811

Downloaded From: https://www.spiedigitallibrary.org/conference-proceedings-of-spie on 10 Mar 2023
Terms of Use: https://www.spiedigitallibrary.org/terms-of-use

photothermal interferometry approach.[2] In particular, our liquid PTS IR sensor consists of a Mach-Zehnder Interferometer (MZI) able to sense sub-nm phase shift $\Delta\varphi$ between its two arms.

Employing a He-Ne as a probe laser and an EC-QCL as an excitation laser, arranged in a dual-beam collinear configuration, we use the resulting spectrometer to target water at trace level in organic solvents and aviation jet-fuel. Reference values for water from a coulometric Karl Fischer (KF) titrator were used as a quantitative reference to calibrate and validate the spectrometer.

2. EXPERIMENTAL SETUP

In detail, a CW HeNe probe laser (nominally 632.8 nm, 1.4 mW power, linear polarized) is used in the MZI. The MZI is built using two 50:50 beam splitters. The probe beam is first split (BS1) into two beams of equal intensity which are then directed through the reference and analyte channel of a liquid flow cell. After the flow cell, the beams are again directed onto a beam splitter (BS2) which creates two interfering output beams of the MZI. Each beam is detected by a silicon photodetector (PD1 and PD2) which are used in a differential configuration.

The PTS pump laser is an external cavity (EC)-QCL tunable from 1730 to 1565 cm^{-1} to target the bending mode (ν_2 ~ 1645 cm^{-1}) of water. A mechanical chopper is used to modulate the pump laser at a frequency f_{mod}. The modulated pump laser beam is focused using a ZnSe lens and directed through the analyte channel using gold covered mirrors. The probe beam and the pump beam are made collinear before the analyte channel by means of a ZnSe dichroic mirror (DM).

The differential photodiode signal (PD1-PD2) of the MZI is demodulated using a lock-in amplifier (LIA) at the pump modulation frequency f_{mod}. The output of the LIA is sent to a data-acquisition card for data recording. The schematic of the experimental setup is depicted in Figure 1. Further details, regarding the used optical components, data acquisition and injection system, can be found in our recent work.[4]

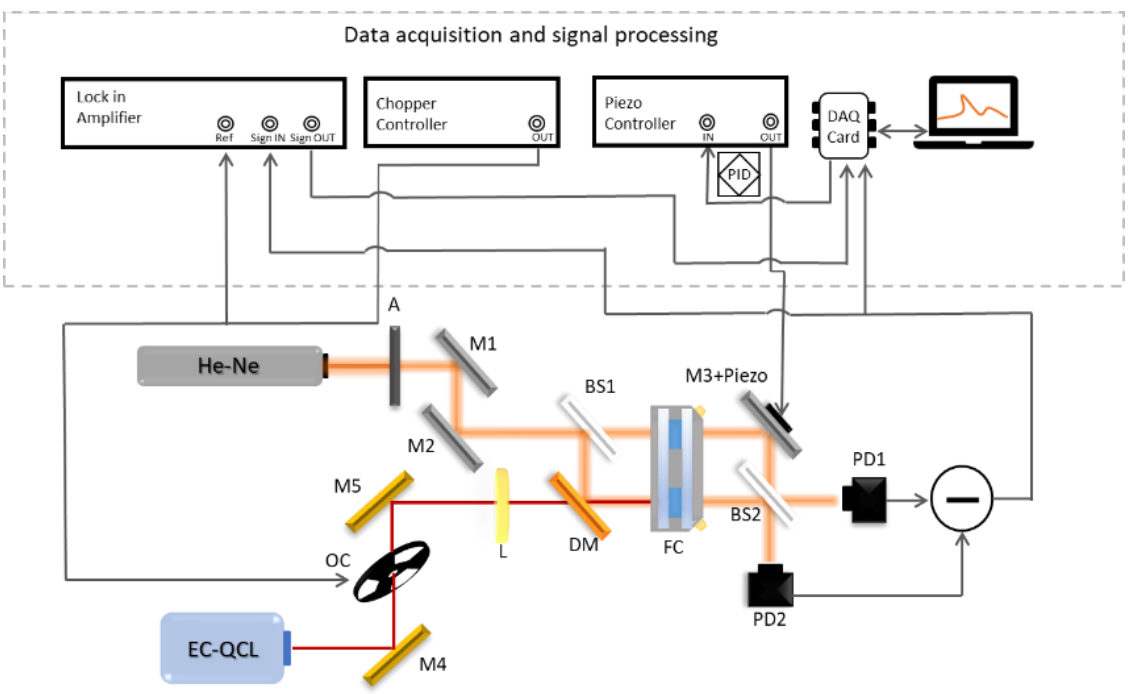

Figure 1. Schematic of PTS-MZI arranged in a dual beam (probe-pump) co-linear configuration. (M1-5…mirrors, L…lens, A…attenuator, OC…optical chopper, BS1-2…beam splitters, DM…dichroic mirror, FC…fluidic cell, PD1-2…Si photodetectors).

It is important to note that both the flow cell and the opto-mechanic components are actively temperature stabilized to reduce thermal drifts (at 22.5 °C). The setup is placed within an enclosure which is constantly flushed with dry air to reduce water vapor contribution as noise source.

Downloaded From: https://www.spiedigitallibrary.org/conference-proceedings-of-spie on 10 Mar 2023
Terms of Use: https://www.spiedigitallibrary.org/terms-of-use

The MZI is held in its quadrature point (=equal intensity in both outputs) using a PID controlled piezo electric transducer (PZT) mounted directly on a mirror in one arm of the MZI (M3). By changing the extension of the piezo, the length of one of the arms of the MZI is slightly adjusted, compensating the phase difference between both arms. When starting a PTS experiment, first the quadrature point of the MZI has to be found: prior to the measurement, both channels of the transmission cell are filled with a reference solution (e.g.: the solvent), the piezo voltage is adjusted manually via the piezo controller to the quadrature point where the intensity onto the two detectors is equal. Once this point has been found the PID is enabled. The response of the PID is set up so that it compensates slow drifts of the MZI but does not attenuate faster changes induced by the modulated pump beam.

Keeping the interferometer locked at the quadrature point has two advantages. First, the signal is maximized at the quadrature point where the interferometer exhibits its highest sensitivity. As shown in Figure 2, the experimental interference pattern was recorded by applying a ramp to the piezo electric actuator via its dedicated SW (ramp gain=60 V, ramp frequency=0.06 Hz). It demonstrates that the two arms of the interferometer are aligned such that a good fringe contrast has been achieved and the interference has been maximized. Second, the MZI response is linear close to the quadrature point but deviates from linearity as the system moves further from it.

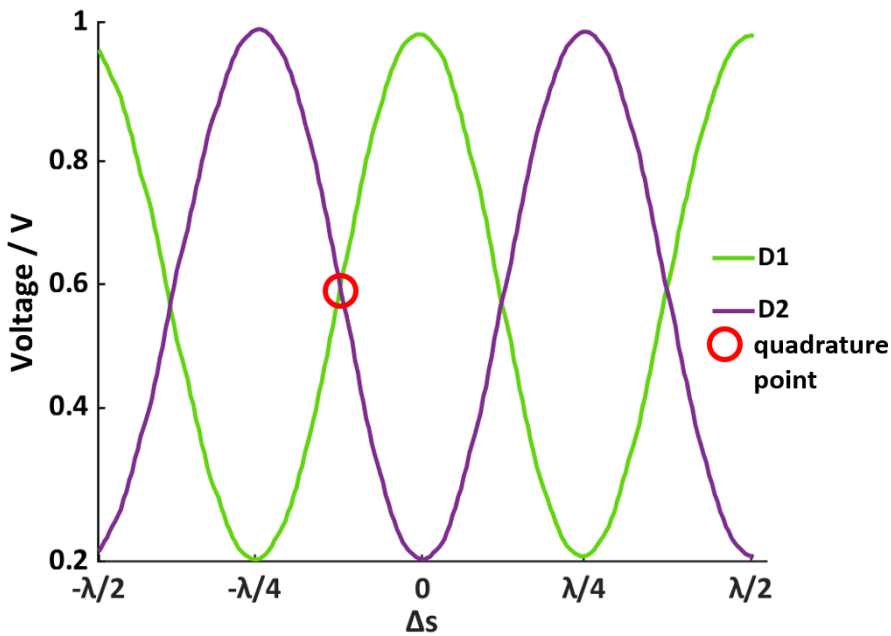

Figure 2. Intensity response on the two detectors at varying phase shift Δφ. The working point, where D1 and D2 exhibit equal intensities, is the so called 'quadrature-point'.

Sample solutions were prepared from solvents and deionized water. As ethanol mixes with water in any ratio, ethanol-water mixtures were prepared by directly mixing known amounts of both components. Chloroform and jet fuel -aprotic and hydrophobic solvents – only dissolve small amounts of water. To make solutions of water in these solvents they were mixed with aliquots of water using an ultrasonic bath. The mixtures were left over-night in a separatory funnel allowing for phase separation. The aqueous phase was then removed. Samples were prepared by mixing water containing solvent with dry solvent. The actual water content in these samples was determined using a coulometric Karl Fischer titrator. PTS measurements were carried out shortly after the KF determination.

For PTS measurements, 30 scans across the full tuning range of the EC-QCL were acquired per each sample and averaged (each scan taking 3 s). In each measurement run first the pure solvent was measured to allow for background removal. To obtain accurate band shapes, the lock-in amplifier demodulated differential signal (PD1-PD2) was subjected, in post-processing, to background removal and laser power normalization. In this way band-shape and absorption peaks' positioning could be compared against the one measured with FTIR transmission spectroscopy.

Downloaded From: https://www.spiedigitallibrary.org/conference-proceedings-of-spie on 10 Mar 2023
Terms of Use: https://www.spiedigitallibrary.org/terms-of-use

3. RESULTS

The recorded mid-IR spectra of water in ethanol, chloroform and aircraft jet-fuel, respectively, are depicted in Figure 3. In all three cases, bands-shape and absorption peaks retrieved via PTS-MZI are in excellent agreement with the ones recorded via transmission FTIR spectrometer.

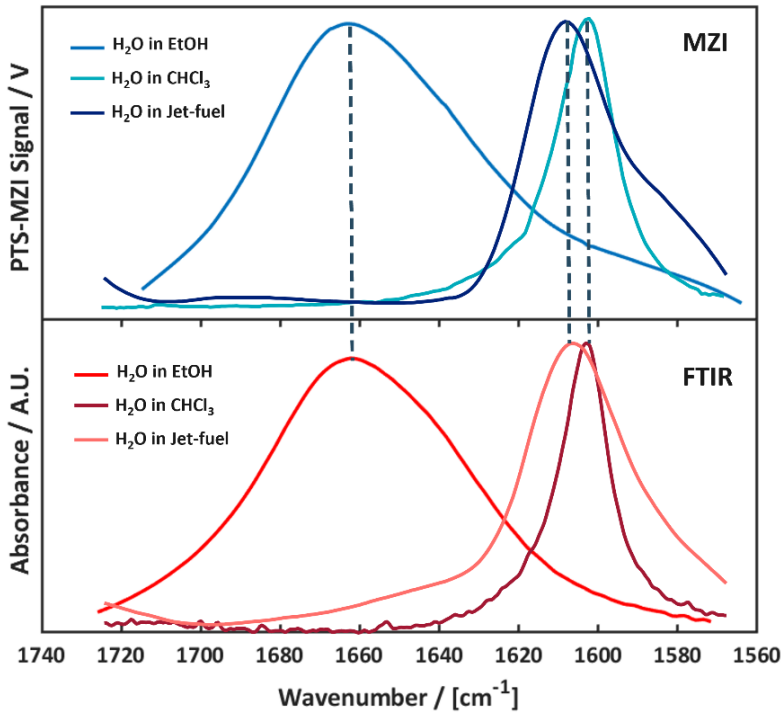

Figure 3. Top panel: Spectra of the H_2O deformation band in EtOH, $CHCl_3$ and jet fuel recorded via PTS-MZI. Bottom panel: Mid-IR spectra of H_2O in EtOH, $CHCl_3$ and jet fuel recorded via FTIR.

By determining reference water concentrations through KF titration, the PTS-MZI spectrometer was calibrated. Recorded calibration curves datapoints are collected in the following Table 1. The sensor exhibits a linear trend within the concentration range for each solvent.

Table 1. Measured calibration curves datapoints targeting water in different matrices via PTS-MZI.

Solvent	Concentrations / %v/v	PTS-MZI Signal / V
Ethanol	0.01	0.628
	0.05	0.634
	0.1	0.643
	0.5	0.696
	1	0.765
Chloroform	0.0001	0.068
	0.009	0.100
	0.02	0.132
	0.051	0.245
Jet-fuel	0.0007	0.485
	0.002	0.494
	0.004	0.504
	0.006	0.517

Downloaded From: https://www.spiedigitallibrary.org/conference-proceedings-of-spie on 10 Mar 2023
Terms of Use: https://www.spiedigitallibrary.org/terms-of-use

Based on these calibrations, LODs and LOQs were determined for water detection in each of the three solvents (see table 2):[5]

Table 2. Calculated LODs and LOQs for water in different matrices via PTS-MZI.

Solvent	LOD (ppm)	LOQ (ppm)
Ethanol	400	1400
Chloroform	7	25
Jet-fuel	20	60

It is worth noticing that the solvents affect the water band shape: depending on the solvent, water exhibits different absorption peak positions (at 1660 cm^{-1} in the case of EtOH, at 1600 cm^{-1} in the case of chloroform and at 1608 cm^{-1} in the case of jet-fuel) and band shapes due to intermolecular interactions.
Seki et al.[6] have described bending mode of water (ν_2 ~ 1645 cm^{-1}) as a powerful tool for the study and analysis of hydrogen bond structures and strength. Indeed, H-O-H bending mode of water-ethanol mixture has been reported to be affected by a small blue shift (1660 cm^{-1}) and a broader band-shape in comparison to the bending mode of pure water.[7–9]
In water-chloroform mixtures, the H-O-H bending mode has been reported to be red shifted and to have significantly narrower band-shape as the hydrogen bonds are disrupted in this solvent.[10] Both these effects are seen in our PTS spectra as well as in the FTIR reference measurements.
In water-jet-fuel mixtures similar effects can be observed as in water-chloroform mixtures (see Figure 3): the water absorption peak is shifted toward lower frequencies and is narrower than in ethanol mixtures or as pure water. The effects on the band position and shape are not as strong as those in chloroform. This effect also has recently been observed in other fuels and biofuels for aircraft turbine engines.[11]

4. INFLUENCE OF MATRIX

As reported in Table 2, LODs and LOQs differ. They are about two orders of magnitude higher in the case of ethanol than in the other two solvents under investigation (chloroform and jet-fuel). Indeed, as per Figure 3, even though the same analyte is measured in all three examples, the analyte's absorption peak shape and position differ based on the matrix and the interactions that occur within the mixture. This is one of the effects affecting the sensitivity, as the PTS signal depends also on the optical power $P(\tilde{\nu})$ provided by the EC-QCL across the spectral region. In EC-QCLs the output power typically is strongly wavelength dependent and lower towards the edges of a laser's tuning range.
Additionally, as depicted by equation (1), the PTS-Signal depends mainly on three parameters: specific heat C_P and density ρ of the solvent and the absorption coefficient of the analyte $\alpha(\tilde{\nu})$. C_P and ρ are similar for both ethanol and chloroform. On the other hand, working at trace-level, the absorption coefficient $\alpha(\tilde{\nu})$ is a combination of both the analyte and the solvent contribution especially in the case in which the solvent itself is already a strong absorber. Indeed, in such a case, the residual optical power for exciting the analyte, is in turn reduced leading to a weaker photothermal effect on the target analyte.
As reported by Figure 4, the absorption coefficient of ethanol is much larger than the one of chloroform in the spectral region covered by the EC-QCL. At the maximum of the water absorption band the absorption of ethanol corresponds to ~ 22.33 cm^{-1}, while the absorption coefficient of chloroform at the maximum of the water absorption band is ~ 0.88 cm^{-1}. It is evident that when targeting water in ethanol, there is a stronger background absorption then in the case of chloroform. In turn, water molecule excitation is reduced in the first case as ethanol molecules absorb more optical power coming from the EC-QCL. This influences the respective LODs and LOQs obtainable in both cases.

Downloaded From: https://www.spiedigitallibrary.org/conference-proceedings-of-spie on 10 Mar 2023
Terms of Use: https://www.spiedigitallibrary.org/terms-of-use

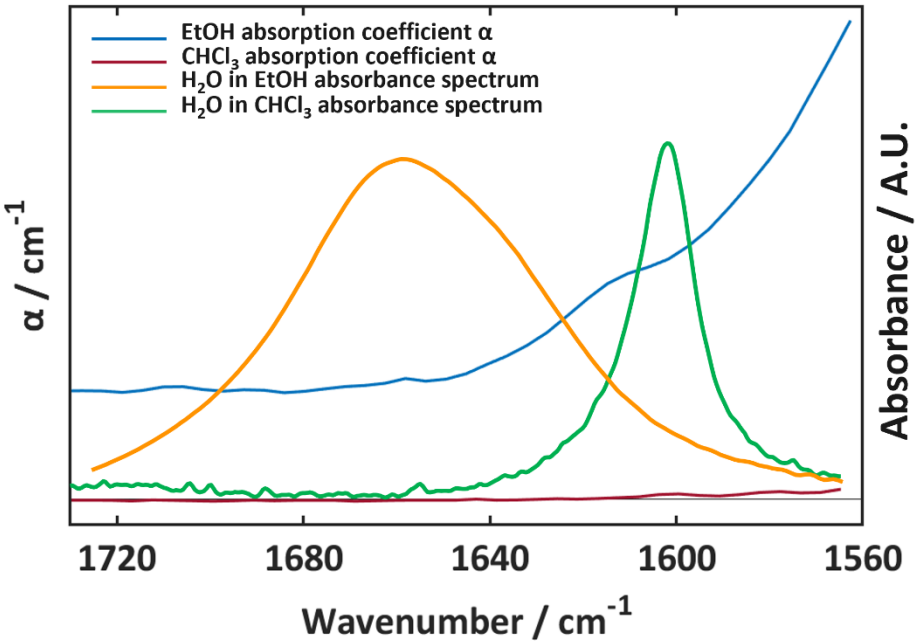

Figure 4. Absorption coefficients of the solvents under investigation within the mid-IR range under analysis – EtOH (blue) and $CHCl_3$ (red) – and mid-IR spectra of water in EtOH (orange) and of water in $CHCl_3$ (green).

5. CONCLUSIONS & OUTLOOK

Using the example of trace water detection in solvents, we have described for the first time a PID-locked photothermal spectrometer based on a Mach Zehnder interferometer for highly sensitive detection of solutes. The photothermal spectra are derived by subtracting the background spectrum from the sample spectrum, normalizing the result to the wavelength dependent power of the used EC-QCL excitation source, and comparing the results to the corresponding absorbance spectra recorded on FTIR spectrometer. The method created is effective both in polar (ethanol) and apolar (chloroform, jet fuel) solvents. We have shown that photothermal spectroscopy can produce results that are highly comparable to those of the gold standard for trace water detection, coulometric KF.

Our results show that the strength of the photothermal effect generation on the target analyte strongly depends on the matrix and background's absorption. Indeed, the sensitivity of water detection depends on the chemical environment of water molecules in the sample. The overall system could be further improved by optimizing the optical pathlength L and the modulation frequency f_{mod} for each solvent and in general, by reducing the noise level, for instance, switching to a fiber-based system or as an advanced miniaturized version of the spectrometer, moving to a MZI on-chip based on integrated waveguides.

6. ACKNOWLEDGMENT

This work has received funding by the European Union's Horizon 2020 research and innovation programme under the Marie Skłodowska-Curie grant agreement No 860808.

REFERENCES

(1) Schwaighofer, A.; Brandstetter, M.; Lendl, B. Quantum Cascade Lasers (QCLs) in Biomedical Spectroscopy. *Chem. Soc. Rev.* **2017**, *46* (19), 5903–5924. https://doi.org/10.1039/C7CS00403F.

(2) Bialkowski, S. E. *Photothermal Spectroscopy Methods for Chemical Analysis*; John Wiley & Sons, 1996.

Downloaded From: https://www.spiedigitallibrary.org/conference-proceedings-of-spie on 10 Mar 2023
Terms of Use: https://www.spiedigitallibrary.org/terms-of-use

(3) Mazzoni, D. L.; Davis, C. C. Trace Detection of Hydrazines by Optical Homodyne Interferometry. *Appl. Opt.* **1991**, *30* (7), 756. https://doi.org/10.1364/AO.30.000756.
(4) Ricchiuti, G.; Dabrowska, A.; Pinto, D.; Ramer, G.; Lendl, B. Dual-Beam Photothermal Spectroscopy Employing a Mach–Zehnder Interferometer and an External Cavity Quantum Cascade Laser for Detection of Water Traces in Organic Solvents. *Anal. Chem.* **2022**, *94* (47), 16353–16360. https://doi.org/10.1021/acs.analchem.2c03303.
(5) *IUPAC. Compendium of Chemical Terminology, 2nd ed. (the "Gold Book"). Compiled by A. D. McNaught and A. Wilkinson. Blackwell Scientific Publications, Oxford (1997). Online version (2019-) created by S. J. Chalk. ISBN 0-9678550-9-8. https://doi.org/10.1351/goldbook.*
(6) Seki, T.; Chiang, K.-Y.; Yu, C.-C.; Yu, X.; Okuno, M.; Hunger, J.; Nagata, Y.; Bonn, M. The Bending Mode of Water: A Powerful Probe for Hydrogen Bond Structure of Aqueous Systems. *J. Phys. Chem. Lett.* **2020**, *11* (19), 8459–8469. https://doi.org/10.1021/acs.jpclett.0c01259.
(7) Yu, X.; Seki, T.; Yu, C.-C.; Zhong, K.; Sun, S.; Okuno, M.; Backus, E. H. G.; Hunger, J.; Bonn, M.; Nagata, Y. Interfacial Water Structure of Binary Liquid Mixtures Reflects Nonideal Behavior. *J. Phys. Chem. B* **2021**, *125* (37), 10639–10646. https://doi.org/10.1021/acs.jpcb.1c06001.
(8) Venables, D. S.; Schmuttenmaer, C. A. Spectroscopy and Dynamics of Mixtures of Water with Acetone, Acetonitrile, and Methanol. *J. Chem. Phys.* **2000**, *113* (24), 11222–11236. https://doi.org/10.1063/1.1328072.
(9) Wright, A. M.; Howard, A. A.; Howard, J. C.; Tschumper, G. S.; Hammer, N. I. Charge Transfer and Blue Shifting of Vibrational Frequencies in a Hydrogen Bond Acceptor. *J. Phys. Chem. A* **2013**, *117* (26), 5435–5446. https://doi.org/10.1021/jp401642b.
(10) Zhou, D.; Wei, Q.; Bian, H.; Zheng, J. Direct Vibrational Energy Transfer in Monomeric Water Probed with Ultrafast Two Dimensional Infrared Spectroscopy. *Chin. J. Chem. Phys.* **2017**, *30* (6), 619–625. https://doi.org/10.1063/1674-0068/30/cjcp1710189.
(11) West, Z. J.; Yamada, T.; Bruening, C. R.; Cook, R. L.; Mueller, S. S.; Shafer, L. M.; DeWitt, M. J.; Zabarnick, S. Investigation of Water Interactions with Petroleum-Derived and Synthetic Aviation Turbine Fuels. *Energy Fuels* **2018**, *32* (2), 1166–1178. https://doi.org/10.1021/acs.energyfuels.7b02844.

Downloaded From: https://www.spiedigitallibrary.org/conference-proceedings-of-spie on 10 Mar 2023
Terms of Use: https://www.spiedigitallibrary.org/terms-of-use